Supplementary Materials

Operational Weather Windows for Offshore Wind in the Taiwan Strait: Long-Term Variability, Regional Wind Modes, and Climate Linkages

S1: ERA5 Comparison with High-Resolution Regional Wind Fields

The overall performance of ERA5 100-m wind speeds at the study point was compared with the 3-km CWA-WRF analyzed fields, generated by CWA's WRF-based data-assimilation system and constrained by local surface and radar observations (Chen et al. 2020). Tseng et al. (2024) previously compared ERA5 with the CWA-WRF analyzed fields and reported correlations exceeding 0.9 over the Taiwan Strait. This study further assessed the direction and magnitude of ERA5 bias relative to wind speed magnitude and its implications for weather-window detection over 2018 - 2023, the overlapping period of the two-dataset availability. The CWA-WRF analyzed fileds were aggregated to the ERA5 0.25° grid cell by averaging all grid points within ±0.125° of the study point, ensuring a consistent spatial footprint between the two datasets.

ERA5 systematically underestimates wind speeds relative to the CWA-WRF analyzed fields (MBE = -0.99 m s^{-1}), with the bias increasing with wind speed magnitude and reaching over -1 m s^{-1} in the threshold-critical 11-13 m s^{-1} range (Fig. S1a), consistent with ERA5's coarser spatial resolution smoothing fine-scale wind speed gradients. Because ERA5 underestimates wind speeds near the 12 m s^{-1} threshold, it systematically overcounts weather windows relative to the high-resolution analyzed fields by a mean of 3.9 counts per month across years (Fig. S1b). This overcounting is most pronounced in autumn and transitional months - peaking in November (+7.7 counts/month) and October (+6.0 counts/month) - and smallest during summer (JJA mean overcount of 2.6 counts/month). Despite this systematic underestimation, ERA5 reliably captures interannual variability in weather-window counts - annual means correlate significantly with the CWA-WRF analyzed fields ($r = 0.903$, $p < 0.05$, $n = 6$ years; Fig. S1c), and JJA seasonal means show equally high agreement ($r = 0.902$, $p < 0.05$; Fig. S1d). Since this study focuses on interannual and lower-frequency variability and its climate linkages rather than absolute counts, the systematic overcount affects all years proportionally and does not alter the statistical relationships identified. Practitioners using ERA5-derived absolute weather-window counts for operational planning should account for this positive bias, particularly during autumn and transitional months.

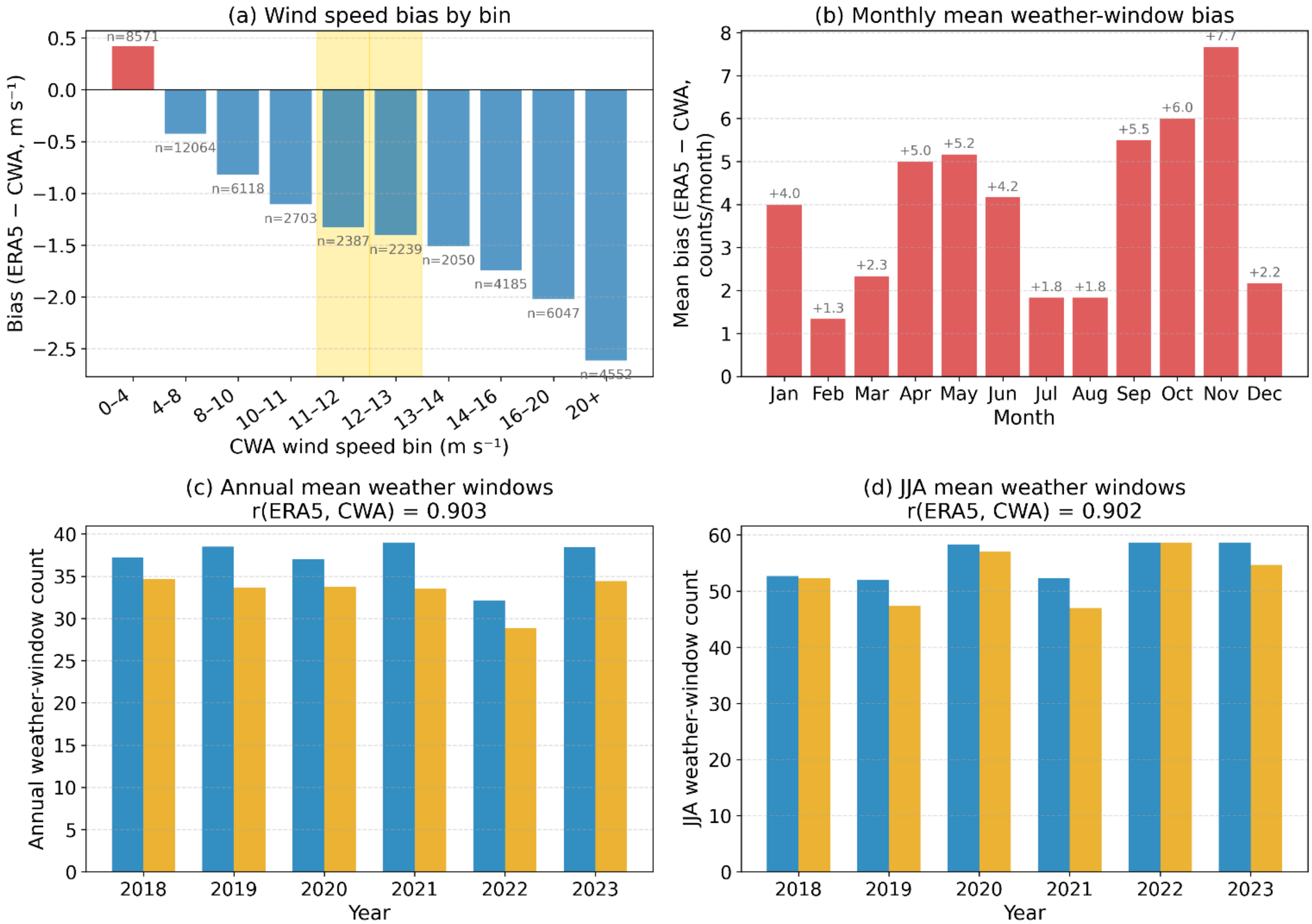

Figure S1: Comparison of ERA5 100-m wind speeds and weather-window counts with the CWA-WRF analyzed fields (shown as CWA, 3 km resolution) at the study point (24° N, 120° E) for 2018-2023. For comparison, CWA wind speeds were aggregated to the ERA5 0.25° grid cell by averaging all grid points within ±0.125° of the study point. (a) Mean bias (MBE, ERA5 - CWA) in wind speed stratified by CWA wind speed bins; gold shading highlights the threshold-critical 11 - 13 m s^{-1} range relevant to 12 m s^{-1} weather-window detection. (b) Mean monthly bias in weather-window counts (ERA5 - CWA). (c) Annual mean weather-window counts for ERA5 (blue) and CWA (orange) with Pearson correlation r. (d) As in (c) but for JJA seasonal means.

S2. Sensitivity of weather-window definitions to wind-speed and wave-height thresholds

The sensitivity of weather-window accessibility to different combinations of wind-speed and significant wave height thresholds, as well as to different required durations, is evaluated in Fig. S2. In general, higher thresholds correspond to greater accessibility, as adverse weather conditions occur less frequently, whereas longer required durations result in lower accessibility because extended calm periods are rarer. Despite differences in magnitude, monthly accessibility exhibits strong coherence across alternative definitions. For instance, correlations between monthly weather-window counts defined using a 12 m s^{-1} wind threshold and a 1.5 m wave-height threshold exceed 0.98, while correlations between wave-only and combined wind–wave criteria exceed 0.99. This robustness supports the use of wind-speed–based criteria as a representative measure of weather-window variability. Accordingly, subsequent analyses adopt the 12 m s^{-1} 100-m wind-speed threshold sustained for 12 hours.

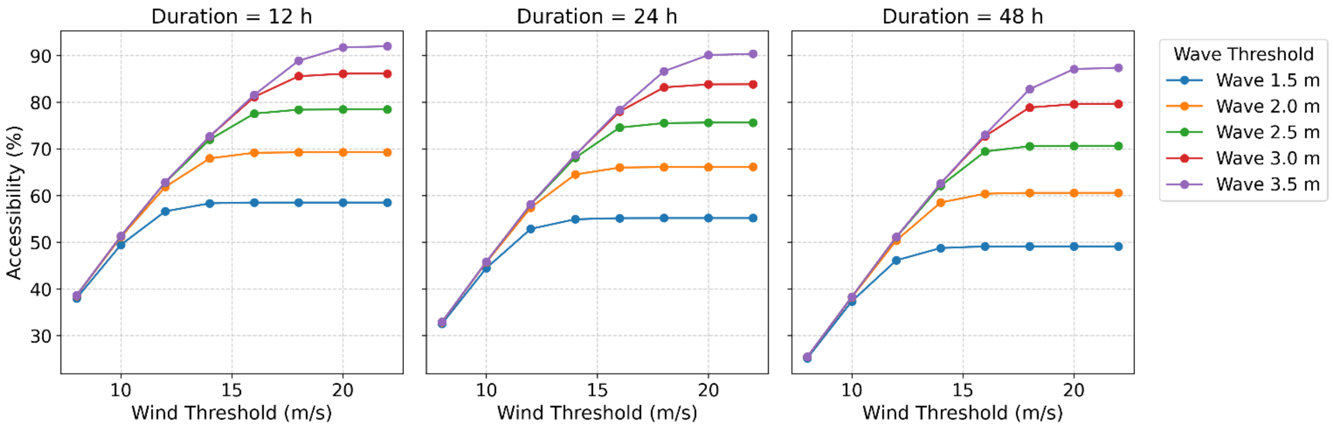

Figure S2: Sensitivity of accessibility (percentage of total time in %) to thresholds of 100-m wind speed and significant wave height during 1960 - 2024. Panels show results for required weather-window durations of 12 h (left), 24 h (middle), and 48 h (right).

S3. Supporting physical diagnostic of EOF1 using 100-m vector-wind anomalies

Because EOF1 shows a coherent wind-speed pattern across the Taiwan Strait, we examined the associated 100-m wind-vector anomalies to assess whether PC1 is accompanied by flow patterns consistent with terrain modification by Taiwan's Central Mountain Range. Figure S3 shows JJA-mean u100 and v100 anomalies regressed onto PC1 using ERA5 data. The shading represents the magnitude of the regressed JJA-mean u100/v100 vector anomaly, calculated as the square root of the sum of the squared u and v regression slopes, rather than the EOF1 wind-speed loading. Therefore, the areas of largest vector-anomaly magnitude are not expected to coincide exactly with the largest EOF1 loadings shown in Fig. 5a.

The regressed vectors show a broad clockwise anomaly pattern over and around the Taiwan Strait, with a stronger westerly component south of Taiwan and more meridional flow along the western side of the island. A local maximum in vector-anomaly magnitude occurs near the western coast of Taiwan, west of the Central Mountain Range axis. This pattern is spatially consistent with terrain-modified flow around Taiwan's topography and suggests that the PC1 wind-speed mode may partly reflect regional flow deflection and acceleration associated with the Central Mountain Range. This regression analysis should be interpreted as a supporting physical diagnostic of the PC1-associated flow geometry rather than as an independent causal test of topographic forcing.

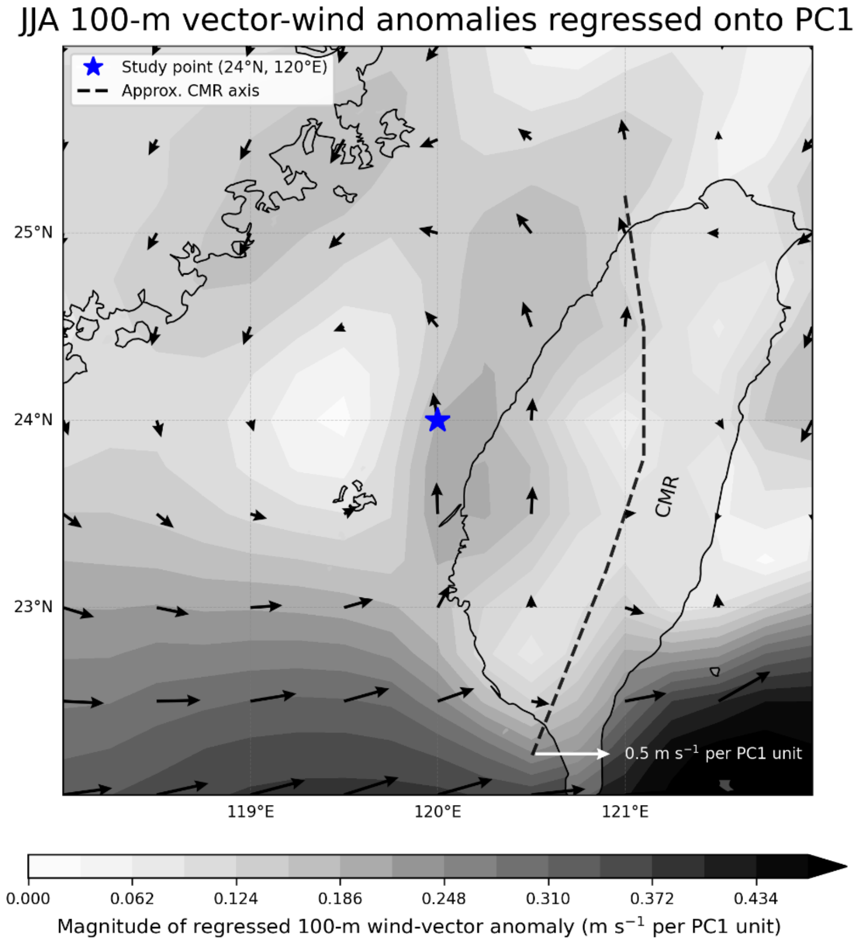

Figure S3. JJA 100-m vector-wind anomalies regressed onto PC1 for 1960–2024. Arrows show the u100 and v100 regression coefficients, and shading shows the magnitude of the regressed wind-vector anomaly. The dashed line marks the approximate axis of Taiwan's Central Mountain Range, and the blue star marks the Taiwan Strait study point. This diagnostic is intended to characterize the PC1-associated flow geometry rather than to independently attribute the mode to topographic forcing.

Table S1: Wind- and wave-limit thresholds for various vessel types and operational functions. Crew-Transfer-Vessel (CTV) data are adapted from Hu et al. (2019); other vessel types follow Moore et al. (2024).

Vessel Type	Function	Wind Limit (10 m, m/s)	Wave Limit (m)
Crew Transfer Vessel (CTV) (from Monohull, Catamaran, Trimaran, SWATH, SES)	O & M access	10	1-2.2

Vessel Type	Function	Wind Limit (10 m, m/s)	Wave Limit (m)
Amplemann	Motion-compensated gangway	20	3
AHTS	Installation of anchors & moorings	20	2
Cable Laying	Installation of Cables	15	3.5
Heavy-lift vessel	Mating of platforms	15	1.8

References

Chen, I.H., Hong, J.-S., Tsai, Y.-T., and Fong, C.-T.: Improving Afternoon Thunderstorm Prediction over Taiwan through 3DVar-Based Radar and Surface Data Assimilation, Weather and Forecasting 35, 2603-2620, https://doi.org/10.1175/WAF-D-20-0037.1, 2020.

Hu, B., Stumpf, P., and van der Deijl, W.: Annual Offshore Wind Access Report (No. 40), TNO, available at: https://publications.tno.nl/publication/34634066/MqvM2m (last access: 26 January 2026), 2019.

Moore, D., Eftekhari, A., and Nash, S.: Weather window analysis for the deployment, operation, and maintenance of marine renewable energy devices in Irish coastal waters, J. Ocean Eng. Mar. Energy, 10, 711–729, https://doi.org/10.1007/s40722-024-00340-2, 2024.

Tseng, W.-L., Lin, C.-W., Wang, Y.-C., Hsu, H.-H., Chiu, K.-M., Wu, Y.-S., Hsieh, Y.-H., and Chen, Y.-T.: Evaluating constraints on offshore wind farm installation across the Taiwan Strait by exploring the influence of El Niño–Southern Oscillation on weather window assessment, Heliyon, 10, e40125, https://doi.org/10.1016/j.heliyon.2024.e40125, 2024.